
Wasserstein Adversarial Examples via Projected Sinkhorn Iterations

Eric Wong¹ Frank R. Schmidt² J. Zico Kolter^{3,4}

Abstract

A rapidly growing area of work has studied the existence of adversarial examples, datapoints which have been perturbed to fool a classifier, but the vast majority of these works have focused primarily on threat models defined by ℓ_p norm-bounded perturbations. In this paper, we propose a new threat model for adversarial attacks based on the Wasserstein distance in image space. In the image classification setting, such distances measure the cost of moving pixel mass, which can naturally represent “standard” image manipulations such as scaling, rotation, translation, and distortion (and can potentially be applied to other settings as well). To generate Wasserstein adversarial examples, we develop a procedure for approximate projection onto the Wasserstein ball, based upon a modified version of the Sinkhorn iteration. The resulting algorithm can successfully attack image classification models, bringing traditional CIFAR10 models down to 3% accuracy within a Wasserstein ball with radius 0.1 (i.e., moving 10% of the image mass 1 pixel), and we demonstrate that PGD-based adversarial training can improve this adversarial accuracy to 76%. In total, this work opens up a new direction of study in adversarial robustness, more formally considering convex metrics that accurately capture the invariances that we typically believe should exist in classifiers, and code for all experiments in the paper is available at <https://github.com/locuslab/projected.sinkhorn>.

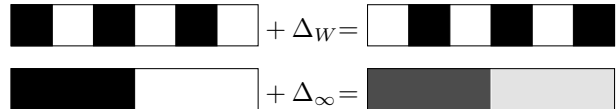


Figure 1. A minimal example exemplifying the difference between Wasserstein perturbations and ℓ_∞ perturbations on an image with six pixels. The top example utilizes a perturbation Δ_W to shift the image one pixel to the right, which is small with respect to 2-Wasserstein distance since each pixel moved a minimal amount ($\|\Delta_W\|_{W_2} = 3$), but large with respect to ℓ_∞ distance since each pixel changed a maximal amount ($\|\Delta_W\|_\infty = 1$). In contrast, the bottom example utilizes a perturbation Δ_∞ which changes all pixels to be grayer by 0.3. This is small with respect to ℓ_∞ distance, since each pixel changes by a small amount ($\|\Delta_\infty\|_\infty = 0.3$), but large with respect to 2-Wasserstein distance, since the mass on each pixel on the left had to move 3 pixels over at a cost of 3^2 per unit of mass ($\|\Delta_\infty\|_W = 8.1$).

1. Introduction

A substantial effort in machine learning research has gone towards studying *adversarial examples* (Szegedy et al., 2014), commonly described as datapoints that are indistinguishable from “normal” examples, but are specifically perturbed to be misclassified by machine learning systems. This notion of indistinguishability, later described as the threat model for attackers, was originally taken to be ℓ_∞ bounded perturbations, which model a small amount of noise injected to each pixel (Goodfellow et al., 2015). Since then, subsequent work on understanding, attacking, and defending against adversarial examples has largely focused on this ℓ_∞ threat model and its corresponding ℓ_p generalization. While the ℓ_p threat model is convenient, it is by no means a comprehensive description of all possible adversarial perturbations. Other work (Engstrom et al., 2017) has looked at perturbations such as rotations and translations, but beyond these specific transforms, there has been little work considering broad, well-defined classes of attacks beyond the ℓ_p ball.

In this paper, we propose a new type of adversarial perturbation that encodes a general class of attacks that is fundamentally different from the ℓ_p ball. Specifically, we propose an attack model where the perturbed examples are bounded in Wasserstein distance in image space¹ from the original

¹Machine Learning Department, Carnegie Mellon University, Pittsburgh, Pennsylvania, USA ²Bosch Center for Artificial Intelligence, Renningen, Germany ³Computer Science Department, Carnegie Mellon University, Pittsburgh, Pennsylvania, USA ⁴Bosch Center for Artificial Intelligence, Pittsburgh, Pennsylvania, USA. Correspondence to: Eric Wong <ericwong@cs.cmu.edu>.

¹This is in contrast to work that considers Wasserstein distances in the training distribution (Sinha et al., 2018).

example. Intuitively, for images, this is the cost of moving around pixel mass to change one image into another. Note that the Wasserstein and ℓ_p ball can be quite different: examples that are close in Wasserstein distance can be quite far in ℓ_p distance, and vice versa (a pedagogical example demonstrating this is in Figure 1).

We develop this idea of Wasserstein adversarial examples in two main ways. Since adversarial examples are typically best generated using variants of projected gradient descent, we first derive an algorithm that projects onto the Wasserstein ball. However, performing an exact projection is computationally expensive, so our main contribution here is to derive a fast method for *approximate* projection. The procedure can be viewed as a modified Sinkhorn iteration, but with a more complex set of update equations. Second, we develop efficient methods for adversarial training under this threat method. Because this involves repeatedly running this projection within an inner optimization loop, speedups that use a *local* transport plan are particularly crucial (i.e. only moving pixel mass to nearby pixels), making the projection complexity linear in the image size.

We evaluate the attack quality on standard models, showing for example that we can reduce the adversarial accuracy of a standard CIFAR10 classifier from 94.7% to 3% using a Wasserstein ball of radius 0.1 (equivalent to moving 10% of the mass of the image by one pixel), whereas the same attack reduces the adversarial accuracy of a model certifiably trained against ℓ_∞ perturbations from 66% to 61%. In contrast, we show that with adversarial training, we are able to improve the adversarial accuracy of this classifier to 76% while retaining a nominal accuracy of 80.7%. We additionally show, however, that existing *certified* defenses cannot be easily extended to this setting; building models provably robust to Wasserstein attacks will require fundamentally new techniques. In total, we believe this work highlights a new direction in adversarial examples: convex perturbation regions which capture a much more intuitive form of structure in their threat model, and which move towards a more “natural” notion of adversarial attacks.

2. Background and Related Work

Much of the work in adversarial examples has focused on the original ℓ_∞ threat model presented by Goodfellow et al. (2015), some of which also extends naturally to ℓ_p perturbations. Since then, there has been a plethora of papers studying this threat model, ranging from improved attacks, heuristic and certified defenses, and verifiers. As there are far too many to discuss here, we highlight a few which are the most relevant to this work.

The most commonly used method for generating adversarial examples is to use a form of projected gradient descent over

the region of allowable perturbations, originally referred to as the Basic Iterative Method (Kurakin et al., 2017). Since then, there has been a back-and-forth of new heuristic defenses followed by more sophisticated attacks. To name a few, distillation was proposed as a defense but was defeated (Papernot et al., 2016; Carlini & Wagner, 2017), realistic transformations seen by vehicles were thought to be safe until more robust adversarial examples were created (Lu et al., 2017; Athalye et al., 2018b), and many defenses submitted to ICLR 2018 were broken shortly after the review period finished (Athalye et al., 2018a). One undefeated heuristic defense is to use the adversarial examples in adversarial training, which has so far worked well in practice (Madry et al., 2018). While traditionally used for ℓ_∞ and ℓ_2 balls (with a natural ℓ_p generalization), in principle, the method can be used to project onto any kind of perturbation region.

Another set of related papers are verifiers and provable defenses, which aim to produce (or train on) certificates that are provable guarantees of robustness against adversarial attacks. Verification methods are now applicable to multi-layer neural networks using techniques ranging from semi-definite programming relaxations (Raghunathan et al., 2018), mixed integer linear programming (Tjeng et al., 2019), and duality (Dvijotham et al., 2018; Wong & Kolter, 2018; Wong et al., 2018). Provable defenses are able to tie verification into training non-trivial deep networks by backpropagating through certificates, which are generated with duality-based bounds (Wong & Kolter, 2018; Wong et al., 2018), abstract interpretations (Mirman et al., 2018), and interval bound propagation (Gowal et al., 2018). These methods have subsequently inspired new heuristic training defenses, where the resulting models can be independently verified as robust (Croce et al., 2018; Xiao et al., 2019). Notably, some of these approaches are *not* overly reliant on specific types of perturbations (e.g. duality-based bounds). Despite their generality, these certificates have only been trained and evaluated in the context of ℓ_∞ and ℓ_2 balls, and we believe this is due in large part to a lack of alternatives.

Highly relevant to this work are attacks that lie outside the traditional ℓ_p ball of imperceptible noise. For example, simple rotations and translations form a fairly limited set of perturbations that can be quite large in ℓ_p norm, but are sometimes sufficient in order to fool classifiers (Engstrom et al., 2017). Other work uses flows to generate spatially transformed adversarial examples, but lacks a well-defined threat model (Xiao et al., 2018) and hasn’t been used in adversarial training. On the other hand, real world adversarial examples do not necessarily conform to the notion of being “imperceptible”, and need to utilize a stronger adversary that is visible to real world systems. Some examples include wearing adversarial 3D printed glasses to fool facial recognition (Sharif et al., 2017), the use of adversarial graffiti to attack traffic sign classification (Eykholt et al.,

2018), and printing adversarial textures on objects to attack image classifiers (Athalye et al., 2018b). While Sharif et al. (2017) allows perturbations that are physical glasses, the others use an ℓ_p threat model with a larger radius, when a different threat model could be a more natural description of adversarial examples that are perceptible on camera.

Last but not least, our paper relies heavily on the Wasserstein distance, which has seen applications throughout machine learning. Used to study monochromatic images in Peleg et al. (1989), the Wasserstein metric has been successfully applied to various vision problems (Rubner et al., 2000; Snow et al., 2016). The traditional Wasserstein distance has the drawback of being computationally expensive: computing a single distance involves solving an optimal transport problem (a linear program) with a number of variables quadratic in the input dimension. However, it was shown that by subtracting an entropy regularization term, one can compute approximate Wasserstein distances extremely quickly using the Sinkhorn iteration (Cuturi, 2013), later shown to run in near-linear time (Altschuler et al., 2017). Our work can be viewed as a special case of unbalanced optimal transport (Chizat et al., 2016), however in the context of projected gradient descent instead of gradient flows. Relevant but orthogonal to our work, is that of Sinha et al. (2018) on achieving distributional robustness. While we both use the Wasserstein distance in the context of adversarial training, the approach is quite different: Sinha et al. (2018) use the Wasserstein distance to perturb the underlying *data distribution*, whereas we use the Wasserstein distance as an attack model for perturbing each *example*.

Contributions This paper takes a step back from using ℓ_p as a perturbation metric, and proposes using the Wasserstein distance instead as an equivalently general but qualitatively different way of generating adversarial examples. To tackle the computational complexity of projecting onto a Wasserstein ball, we use ideas from the Sinkhorn iteration (Cuturi, 2013) to derive a fast method for an approximate projection. Specifically, we show that subtracting a similar entropy-regularization term to the projection problem results in a Sinkhorn-like algorithm, and using local transport plans makes the procedure tractable for generating adversarial images. In contrast to ℓ_∞ and ℓ_2 perturbations, we find that the Wasserstein metric generates adversarial examples whose perturbations have inherent structure reflecting the actual image itself (see Figure 2 for a comparison). We demonstrate the efficacy of this attack on standard models, models trained against this attack, and provably robust models (against ℓ_∞ attacks) on MNIST and CIFAR10 datasets. While the last of these models are not trained to be robust against this attack, we observe that some (but not all) robustness empirically transfers over to protection against the Wasserstein attack. More importantly, we show that while

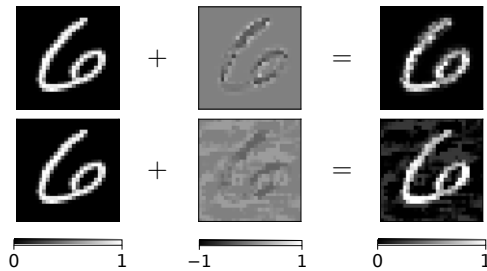


Figure 2. A comparison of a Wasserstein (top) vs an ℓ_∞ (bottom) adversarial example for an MNIST classifier (for $\epsilon = 0.4$ and 0.3 respectively), showing the original image (left), the added perturbation (middle), and the perturbed image (right). Both examples are misclassified as zero. We find that the Wasserstein perturbation has a structure reflecting the actual content of the image, whereas the ℓ_∞ perturbation also attacks the background pixels.

the Wasserstein ball does fit naturally into duality based frameworks for generating and training against certificates, there is a fundamental roadblock preventing these methods from generating non-vacuous bounds on Wasserstein balls.

3. Preliminaries

PGD-based adversarial attacks The most common method of creating adversarial examples is to use a variation of projected gradient descent. Specifically, let (x, y) be a datapoint and its label, and let $\mathcal{B}(x, \epsilon)$ be some ball around x with radius ϵ (the threat model for the adversary). We first define the projection operator onto $\mathcal{B}(x, \epsilon)$ to be

$$\text{proj}_{\mathcal{B}(x, \epsilon)}(w) = \arg \min_{z \in \mathcal{B}(x, \epsilon)} \|w - z\|_2^2 \quad (1)$$

which finds the point closest (in Euclidean space²) to the input w that lies within the ball $\mathcal{B}(x, \epsilon)$. Then, for some step size α and some loss ℓ (e.g. cross-entropy loss), the algorithm consists of the following iteration:

$$x^{(t+1)} = \text{proj}_{\mathcal{B}(x, \epsilon)} \left(x^{(t)} + \arg \max_{\|v\| \leq \alpha} v^T \nabla \ell(x^{(t)}, y) \right) \quad (2)$$

where $x^{(0)} = x$ or any randomly initialized point within $\mathcal{B}(x, \epsilon)$. This is sometimes referred to as projected *steepest* descent, which is used to generate adversarial examples since the standard gradient steps are typically too small. If we consider the ℓ_∞ ball $\mathcal{B}_\infty(x, \epsilon) = \{x + \Delta : \|\Delta\|_\infty \leq \epsilon\}$ and use steepest descent with respect to the ℓ_∞ norm, then we recover the Basic Iterative Method originally presented by Kurakin et al. (2017).

²The use of Euclidean metric in the objective is specific to the setting of projected gradient descent, irrespective of the set $\mathcal{B}(x, \epsilon)$ being projected onto. Proximal operators with respect to Wasserstein instead of Euclidean distances are used in gradient flow problems (Jordan et al., 1998; Peyré, 2015), but are not relevant to our setting.

Algorithm 1 An epoch of adversarial training for a loss function ℓ , classifier f_θ with parameters θ , and step size parameter α for some ball \mathcal{B} .

```

input: Training data  $(x_i, y_i), i = 1 \dots n$ 
for  $i = 1 \dots n$  do
    // Run PGD adversary
     $x_{adv} := x_i$ 
    for  $t = 1 \dots T$  do
         $\delta := \arg \max_{\|v\| \leq \alpha} v^T \nabla \ell(x_{adv}, y_i)$ 
         $x_{adv} := \text{proj}_{\mathcal{B}(x_i, \epsilon)}(x_{adv} + \delta)$ 
    end for
    // Backpropagate with  $x_{adv}$ , e.g. with SGD
    Update  $\theta$  with  $\nabla \ell(f_\theta(x_{adv}), y_i)$ 
end for
    
```

Adversarial training One of the heuristic defenses that works well in practice is to use adversarial training with a PGD adversary. Specifically, instead of minimizing the loss evaluated at a example x , we minimize the loss on an adversarially perturbed example x_{adv} , where x_{adv} is obtained by running the projected gradient descent attack for the ball $\mathcal{B}(x, \epsilon)$ for some number of iterations, as shown in Algorithm 1. Taking $\mathcal{B}(x, \epsilon)$ to be an ℓ_∞ ball recovers the procedure used by Madry et al. (2018).

4. Wasserstein Adversarial Examples

The crux of this work relies on offering a fundamentally different type of adversarial example from typical, ℓ_p perturbations: the Wasserstein adversarial example. Informally, for images, these are examples that have been perturbed by moving pixel mass short distances. Unlike ℓ_p balls, this includes standard image transformations (rotations, translations, distortions), making the Wasserstein distance a more natural metric for images in both monochromatic and RGB image problems (Peleg et al., 1989; Rubner et al., 2000).

4.1. Wasserstein distance

We first define the most crucial component of this work, an alternative metric to ℓ_p distances. The Wasserstein distance (also known as the Earth mover’s distance) is an optimal transport problem that can be understood in the context of distributions as the minimum cost of moving probability mass to change one distribution into another. When applied to images, this can be interpreted as the cost of moving pixel mass from one pixel to another, where the cost increases with pixel distance.

More specifically, let $x, y \in \mathbb{R}_+^n$ be non-negative data points such that $\sum_i x_i = \sum_j y_j = 1$, so images and other inputs need to be normalized, and let $C \in \mathbb{R}_+^{n \times n}$ be some non-negative cost matrix where C_{ij} encodes the cost of moving mass from x_i to y_j (e.g. the distance between two pixels).

Then, the Wasserstein distance $d_W(x, y)$ is defined to be

$$d_W(x, y) = \min_{\Pi \in \mathbb{R}_+^{n \times n}} \langle \Pi, C \rangle \quad (3)$$

subject to $\Pi \mathbf{1} = x, \Pi^T \mathbf{1} = y$

where the minimization is over transport plans Π , whose entries Π_{ij} encode how much mass moves from x_i to y_j . Then, we can define the Wasserstein ball with radius ϵ as

$$\mathcal{B}_W(x, \epsilon) = \{y : d_W(x, y) \leq \epsilon, y \geq 0\} \quad (4)$$

4.2. Projection onto the Wasserstein Ball

In order to generate Wasserstein adversarial examples, we can run the projected gradient descent attack from Equation (2), dropping in the Wasserstein ball \mathcal{B}_W from Equation (4) in place of \mathcal{B} . However, while projections onto regions such as ℓ_∞ and ℓ_2 balls are straightforward and have closed form solutions, simply computing the Wasserstein distance itself requires solving an optimization problem. Thus, the first natural requirement to generating Wasserstein adversarial examples is to derive an *efficient* way to project onto the Wasserstein ball. Specifically, projecting w onto a Wasserstein ball around x with radius ϵ and transport cost matrix C can be written as the following optimization problem:

$$\begin{aligned} & \text{minimize}_{z \in \mathbb{R}_+^n, \Pi \in \mathbb{R}_+^{n \times n}} \frac{1}{2} \|w - z\|_2^2 \\ & \text{subject to } \Pi \mathbf{1} = x, \Pi^T \mathbf{1} = z \\ & \quad \langle \Pi, C \rangle \leq \epsilon \end{aligned} \quad (5)$$

While we could directly solve this optimization problem (using an off-the-shelf quadratic programming solver), this is prohibitively expensive to do for every iteration of projected gradient descent, especially since there is a quadratic number of variables. However, Cuturi (2013) showed that the standard Wasserstein distance problem from Equation (3) can be approximately solved efficiently by subtracting an entropy regularization term on the transport plan W , and using the Sinkhorn-Knopp matrix scaling algorithm. Motivated by these results, instead of solving the projection problem in Equation (5) exactly, the key contribution that allows us to do the projection efficiently is to instead solve the following entropy-regularized projection problem:

$$\begin{aligned} & \text{minimize}_{z \in \mathbb{R}_+^n, \Pi \in \mathbb{R}_+^{n \times n}} \frac{1}{2} \|w - z\|_2^2 + \frac{1}{\lambda} \sum_{ij} \Pi_{ij} \log(\Pi_{ij}) \\ & \text{subject to } \Pi \mathbf{1} = x, \Pi^T \mathbf{1} = z \\ & \quad \langle \Pi, C \rangle \leq \epsilon. \end{aligned} \quad (6)$$

Although this is an *approximate* projection onto the Wasserstein ball, importantly, the looseness in the approximation is only in finding the projection z which is closest (in ℓ_2 norm)

to the original example x . All feasible points, including the optimal solution, are still within the actual ϵ -Wasserstein ball, so examples generated using the approximate projection are still within the Wasserstein threat model. Using the method of Lagrange multipliers, we can introduce dual variables (α, β, ψ) and derive an equivalent dual problem in Lemma 1 (the proof is deferred to Appendix A.1).

Lemma 1. *The dual of the entropy-regularized Wasserstein projection problem in Equation (6) is*

$$\underset{\alpha, \beta \in \mathbb{R}^n, \psi \in \mathbb{R}_+}{\text{maximize}} \quad g(\alpha, \beta, \psi) \quad (7)$$

where

$$g(\alpha, \beta, \psi) = -\frac{1}{2\lambda} \|\beta\|_2^2 - \psi\epsilon + \alpha^T x + \beta^T w - \sum_{ij} \exp(\alpha_i) \exp(-\psi C_{ij} - 1) \exp(\beta_j) \quad (8)$$

Note that the dual problem here differs from the traditional dual problem for Sinkhorn iterates by having an additional quadratic term on β and an additional dual variable ψ . Nonetheless, we can still derive a Sinkhorn-like algorithm by performing block coordinate ascent over the dual variables (the full derivation can be found in Appendix A.3). Specifically, maximizing g with respect to α results in

$$\arg \max_{\alpha_i} g(\alpha, \beta, \psi) = \log(x_i) - \log\left(\sum_j \exp(-\psi C_{ij} - 1) \exp(\beta_j)\right), \quad (9)$$

which is identical (up to a log transformation of variables) to the original Sinkhorn iterate proposed in Cuturi (2013). The maximization step for β can also be done analytically with

$$\arg \max_{\beta_j} g(\alpha, \beta, \psi) = \lambda w_j - W\left(\lambda \exp(\lambda w_j) \sum_i \exp(\alpha_i) \exp(-\psi C_{ij} - 1)\right) \quad (10)$$

where W is the Lambert W function, which is defined as the inverse of $f(x) = xe^x$. Finally, since ψ cannot be solved for analytically, we can perform the following Newton step

$$\psi' = \psi - t \cdot \frac{\partial g / \partial \psi}{\partial^2 g / \partial \psi^2} \quad (11)$$

where

$$\begin{aligned} \partial g / \partial \psi &= -\epsilon + \sum_{ij} \exp(\alpha_i) C_{ij} \exp(-\psi C_{ij}) \exp(\beta_j) \\ \partial^2 g / \partial \psi^2 &= -\sum_{ij} \exp(\alpha_i) C_{ij}^2 \exp(-\psi C_{ij}) \exp(\beta_j) \end{aligned} \quad (12)$$

Algorithm 2 Projected Sinkhorn iteration to project x onto the ϵ Wasserstein ball around y . We use \cdot to denote element-wise multiplication. The log and exp operators also apply element-wise.

input: $x, w \in \mathbb{R}^n, C \in \mathbb{C}^{n \times n}, \lambda \in \mathbb{R}$
 Initialize $\alpha_i, \beta_i := \log(1/n)$ for $i = 1, \dots, n$ and $\psi := 1$
 $u, v := \exp(\alpha), \exp(\beta)$
while α, β, ψ not converged **do**
 // update K
 $K_\psi := \exp(-\psi C - 1)$

 // block coordinate descent iterates
 $\alpha := \log(x) - \log(K_\psi v)$
 $u := \exp(\alpha)$
 $\beta := \lambda w - W(u^T K_\psi \cdot \lambda \exp(\lambda w))$
 $v := \exp(\beta)$

 // Newton step
 $g := -\epsilon + u^T (C \cdot K_\psi) v$
 $h := -u^T (C \cdot C \cdot K_\psi) v$

 // ensure $\psi \geq 0$
 $\alpha := 1$
 while $\psi - \alpha g / h < 0$ **do**
 $\alpha := \alpha / 2$
 end while
 $\psi := \psi - \alpha g / h$
end while
return: $w - \beta / \lambda$

and where t is small enough such that $\psi' \geq 0$. Once we have solved the dual problem, we can recover the primal solution (to get the actual projection), which is described in Lemma 2 and proved in Appendix A.2.

Lemma 2. *Suppose $\alpha^*, \beta^*, \psi^*$ maximize the dual problem g in Equation (8). Then,*

$$\begin{aligned} z_i^* &= w_i - \beta_i / \lambda \\ \Pi_{ij}^* &= \exp(\alpha_i^*) \exp(-\psi^* C_{ij} - 1) \exp(\beta_j^*) \end{aligned} \quad (13)$$

are the corresponding solutions that minimize the primal problem in Equation (6).

The whole algorithm can then be vectorized and implemented as Algorithm 2, which we call projected Sinkhorn iterates. The algorithm uses a simple line search to ensure that the constraint $\psi \geq 0$ is not violated. Each iteration has $8 O(n^2)$ operations (matrix-vector product or matrix-matrix element-wise product), in comparison to the original Sinkhorn iteration which has 2 matrix-vector products. A full derivation of the algorithm and an explanation of how this is can be interpreted as a matrix-scaling algorithm can be found in Appendix A.3.

Table 1. Classification accuracies for models used in the experiments.

DATA SET	MODEL	NOMINAL ACCURACY
MNIST	STANDARD	98.90%
	BINARIZE	98.73%
	ROBUST	98.20%
	ADV. TRAINING	96.95%
CIFAR10	STANDARD	94.70%
	ROBUST	66.33%
	ADV. TRAINING	80.69%

4.3. Local Transport Plans

The quadratic runtime dependence on input dimension can grow quickly, and this is especially true for images. Rather than allowing transport plans to move mass to and from any pair of pixels, we instead restrict the transport plan to move mass only within a $k \times k$ region of the originating pixel, similar in spirit to a convolutional filter. As a result, the cost matrix C only needs to define the cost within a $k \times k$ region, and we can utilize tools used for convolutional filters to efficiently apply the cost to each $k \times k$ region. This reduces the computational complexity of each iteration from $O(n^2)$ to $O(nk^2)$. For images with more than one channel, we can use the same cost matrix for each channel and only allow transport within a channel, so the cost matrix remains $k \times k$. For 5×5 local transport plans on CIFAR10, the projected Sinkhorn iterates typically converge in around 30-40 iterations, taking about 0.02 seconds per iteration on a Titan X for minibatches of size 100. Note that if we use a cost matrix C that reflects the 1-Wasserstein distance, then this problem could be solved even more efficiently using Kantorovich duality, however we use our formulation to enable more general p -Wasserstein distances, or even non-standard cost matrices.

Projected gradient descent on the Wasserstein ball

With local transport plans, the method is fast enough to be used within a projected gradient descent routine to generate adversarial examples on images, and further used for adversarial training as in Algorithm 1 (using steepest descent with respect to ℓ_∞ norm), except that we do an approximate projection onto the Wasserstein ball using Algorithm 2.

5. Results

In this section, we run the Wasserstein examples through a range of typical experiments in the literature of adversarial examples. Table 1 summarizes the nominal error rates obtained by all considered models. All experiments can be run on a single GPU, and all code for the experiments is available at <https://github.com/locuslab/projected-sinkhorn>.

Architectures For MNIST we used the convolutional ReLU architecture used in Wong & Kolter (2018), with two convolutional layers with 16 and 32 4×4 filters each, followed by a fully connected layer with 100 units, which achieves a nominal accuracy of 98.89%. For CIFAR10 we focused on the standard ResNet18 architecture (He et al., 2016), which achieves a nominal accuracy of 94.76%.

Hyperparameters For all experiments in this section, we focused on using 5×5 local transport plans for the Wasserstein ball, and used an entropy regularization constant of 1000 for MNIST and 3000 for CIFAR10. The cost matrix used for transporting between pixels is taken to be the 2-norm of the distance in pixel space (e.g. the cost of going from pixel (i, j) to (k, l) is $\sqrt{|i - k|^2 + |j - l|^2}$), which makes the optimal transport cost a metric more formally known as the 1-Wasserstein distance. For more extensive experiments on using different sizes of transport plans, different regularization constants, and different cost matrices, we direct the reader to Appendix C.

Evaluation at test time We use the following evaluation procedure to attack models with projected gradient descent on the Wasserstein ball. For each MNIST example, we start with $\epsilon = 0.3$ and increase it by a factor of 1.1 every 10 iterations until either an adversarial example is found or until 200 iterations have passed, allowing for a maximum perturbation radius of $\epsilon = 2$. For CIFAR10, we start with $\epsilon = 0.001$ and increase it by a factor of 1.17 until either an adversarial example is found or until 400 iterations have passed, with a maximum perturbation radius of $\epsilon = 0.53$.

5.1. MNIST

For MNIST, we consider a standard model, a model with binarization, a model provably robust to ℓ_∞ perturbations of at most $\epsilon = 0.1$, and an adversarially trained model. Figure 3 contains a visual comparison of Wasserstein adversarial examples generated for each model. The susceptibility of each model to the Wasserstein attack is plotted in Figure 4.

Standard model and binarization For MNIST, despite restricting the transport plan to local 5×5 regions, a standard model is easily attacked by Wasserstein adversarial examples. In Figure 4, we see that Wasserstein attacks with $\epsilon = 0.5$ can successfully attack a typical MNIST classifier 50% of the time, which goes up to 94% for $\epsilon = 1$. A Wasserstein radius of $\epsilon = 0.5$ can be intuitively understood as moving 50% of the pixel mass over by 1 pixel, or alternatively moving less than 50% of the pixel mass more than 1 pixel. Furthermore, while preprocessing images with binarization is often seen as a way to trivialize adversarial examples on MNIST, we find that it performs only marginally better than the standard model against Wasserstein perturbations.

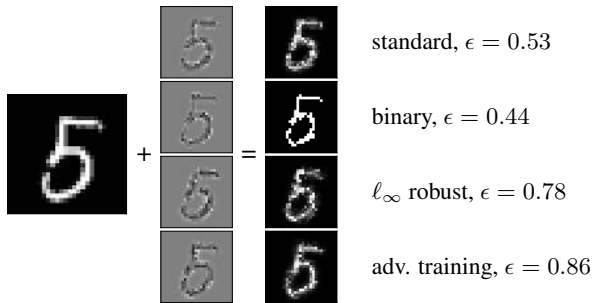


Figure 3. Wasserstein adversarial examples on the MNIST dataset for the four models. Note that the ℓ_∞ robust and the adversarially trained models require a much larger ϵ radius for the Wasserstein ball in order to generate an adversarial example. Each model classifies the corresponding perturbed example as an 8 instead of a 5, except for the first one which classifies as a 6.

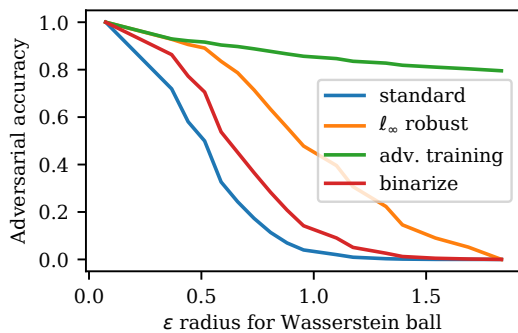


Figure 4. Adversarial accuracy of various models on MNIST when attacked by a Wasserstein adversary over varying sizes of ϵ -Wasserstein balls. We find that all models not trained with adversarial training against this attack eventually achieve 0% accuracy, however we do observe that models trained to be provably robust against ℓ_∞ perturbations are still somewhat more robust than both standard models and models utilizing binarization as a defense.

ℓ_∞ robust model We also run the attack on the model trained by Wong et al. (2018), which is guaranteed to be provably robust against ℓ_∞ perturbations with $\epsilon \leq 0.1$. While not specifically trained against Wasserstein perturbations, in Figure 4 we find that it is substantially more robust than either the standard or the binarized model, requiring a significantly larger ϵ to have the same attack success rate.

Adversarial training Finally, we apply this attack as an inner procedure within an adversarial training framework. To save on computation, during training we adopt a weaker adversary and use 50 iterations of projected gradient descent. We also let ϵ grow within a range and train on the first adversarial example found (essentially a budget version of the attack used at test time). Details regarding this ϵ schedule and also the learning parameters used are in Appendix B.1. We find that the adversarially trained model is empirically the most well defended against this attack of all four models, and cannot be attacked down to 0% accuracy (Figure 4).

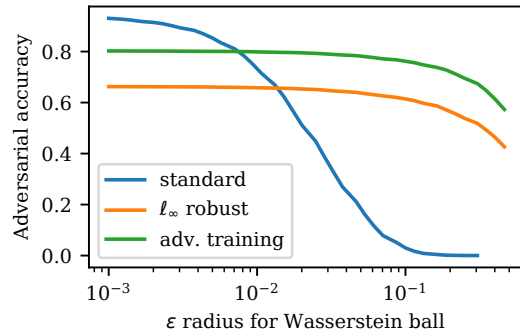


Figure 5. Adversarial accuracy of various models on the CIFAR10 dataset when attacked by a Wasserstein adversary, with the adversarially trained networks being the most robust at $\epsilon = 0.1$.

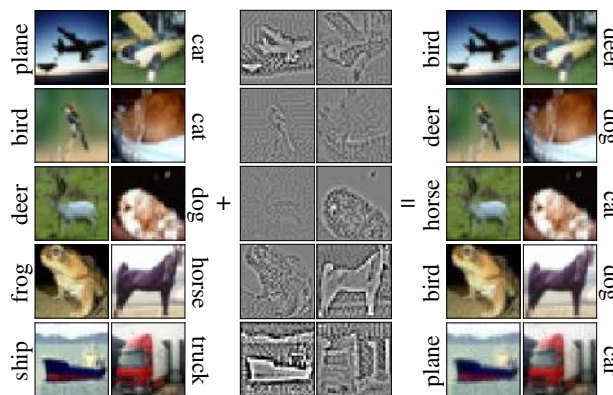


Figure 6. Wasserstein adversarial examples for CIFAR10 on a typical ResNet18 for all 10 classes. The perturbations here represents the total change across all three channels, where total change is plotted within the range ± 0.165 (the maximum total change observed in a single pixel) for images scaled to $[0,1]$.

5.2. CIFAR10

For CIFAR10, we consider a standard model, a model provably robust to ℓ_∞ perturbations of at most $\epsilon = 2/255$, and an adversarially trained model. We plot the susceptibility of each model to the Wasserstein attack in Figure 5.

Standard model We find that for a standard ResNet18 CIFAR10 classifier, a perturbation radius of as little as 0.01 is enough to misclassify 25% of the examples, while a radius of 0.1 is enough to fool the classifier 97% of the time (Figure 5). Despite being such a small ϵ , we see in Figure 6 that the structure of the perturbations still reflect the actual content of the images, though certain classes require larger magnitudes of change than others. Targeted attacks succeed 95% of the time for all target classes at $\epsilon = 0.5$.

ℓ_∞ robust model We further empirically evaluate the attack on a model that was trained to be provably robust against ℓ_∞ perturbations. We use the model from Wong et al. (2018), which is trained to be provably robust against

ℓ_∞ perturbations of at most $\epsilon = 2/255$. Further note that this CIFAR10 model actually is a smaller ResNet than the ResNet18 architecture considered in this paper, and consists of 4 residual blocks with 16, 16, 32, and 64 filters. Nonetheless, we find that while the model suffers from poor nominal accuracy (achieving only 66% accuracy on unperturbed examples as noted in Table 1), the robustness against ℓ_∞ attacks remarkably seems to transfer quite well to robustness against Wasserstein attacks in the CIFAR10 setting, achieving 61% adversarial accuracy for $\epsilon = 0.1$ in comparison to 3% for the standard model.

Adversarial training For CIFAR10, we use a similar scheme that was used for MNIST: we adopt a weaker adversary that uses 50 iterations of projected gradient descent during training and allow ϵ to grow (specific details can be found in Appendix B.2). We find that adversarial training here is also able to defend against this attack, and at the same threshold of $\epsilon = 0.1$, we find that the adversarial accuracy has been improved from 3% to 76%.

5.3. Provable Defenses against Wasserstein Perturbations

Lastly, we present some analysis on how this attack fits into the context of provable defenses, along with a negative result demonstrating a fundamental gap that needs to be solved. The Wasserstein attack can be naturally incorporated into duality based defenses: Wong et al. (2018) show that to use their certificates to defend against other inputs, one only needs to solve the following optimization problem:

$$\max_{x \in B(x, \epsilon)} -x^T y \quad (14)$$

for some constant vector y and for some perturbation region $B(x, \epsilon)$ (a similar approach can be taken to adapt the dual verification from Dvijotham et al. (2018)). For the Wasserstein ball, this is highly similar to the problem of projecting onto the Wasserstein ball from Equation (6), with a linear objective instead of a quadratic objective and fewer variables. In fact, a Sinkhorn-like algorithm can be derived to solve this problem, which ends up being a simplified version of Algorithm 2 (this is shown in Appendix D).

However, there is a fundamental obstacle towards generating provable certificates against Wasserstein attacks: these defenses (and many other, non-duality based approaches) depend heavily on propagating interval bounds from the input space through the network, in order to efficiently bound the output of ReLU units. This concept is inherently at odds with the notion of Wasserstein distance: a “small” Wasserstein ball can use a low-cost transport plan to move all the mass at a single pixel to its neighbors, or vice versa. As a result, when converting a Wasserstein ball to interval constraints, the interval bounds immediately become vacuous:

each individual pixel can attain their minimum or maximum value under some ϵ cost transport plan. In order to guarantee robustness against Wasserstein adversarial attacks, significant progress must be made to overcome this limitation.

6. Conclusion

In this paper, we have presented a new, general threat model for adversarial examples based on the Wasserstein distance, a well-defined metric that captures a kind of perturbation that is fundamentally different from traditional ℓ_p perturbations. To generate these examples, we derived an algorithm for fast, approximate projection onto the Wasserstein ball that exploits local transport plans on images. We successfully attacked standard networks, showing that these adversarial examples are structurally perturbed according to the content of the image, and demonstrated the empirical effectiveness of adversarial training under this threat model. Finally, we observed that provably robust networks (to ℓ_∞ attacks) are more robust than the standard networks against Wasserstein attacks, however we show that the current state of provable defenses is insufficient to directly apply to the Wasserstein ball due to their reliance on interval bounds.

We believe overcoming this roadblock is crucial to the development of verifiers or provable defenses against not just the Wasserstein attack, but also to improve the robustness of classifiers against other attacks that do not naturally convert to interval bounds (e.g. ℓ_0 or ℓ_1 attacks). Whether we can develop efficient verification or provable training methods that do not rely on interval bounds remains an open question.

Perhaps the most natural future direction for this work is to begin to understand the properties of Wasserstein adversarial examples and what we can do to mitigate them, even if only at a heuristic level. However, at the end of the day, the Wasserstein threat model defines just one example of a convex region capturing structure that is different from ℓ_p balls. By no means have we characterized all reasonable adversarial perturbations, and so a significant gap remains in determining how to rigorously define general classes of adversarial examples that can characterize natural phenomena different from the ℓ_p and Wasserstein balls.

Finally, although we focused primarily on adversarial examples, the method of projecting onto Wasserstein balls may be applicable outside of deep learning. Projection operators play a major role in optimization algorithms beyond projected gradient descent (e.g. ADMM and alternating projections). Even more generally, the techniques in this paper could be used to derive Sinkhorn-like algorithms for classes of problems that consider Wasserstein constrained variables. Lastly, while the projected Sinkhorn iteration is guaranteed to converge, deriving specific rates of convergence similar to the original Sinkhorn iteration is an open problem.

References

- Altschuler, J., Weed, J., and Rigollet, P. Near-linear time approximation algorithms for optimal transport via sinkhorn iteration. In *Advances in Neural Information Processing Systems*, pp. 1964–1974, 2017.
- Athalye, A., Carlini, N., and Wagner, D. Obfuscated gradients give a false sense of security: Circumventing defenses to adversarial examples. In *Proceedings of the 35th International Conference on Machine Learning, ICML 2018*, July 2018a. URL <https://arxiv.org/abs/1802.00420>.
- Athalye, A., Engstrom, L., Ilyas, A., and Kwok, K. Synthesizing robust adversarial examples. In Dy, J. and Krause, A. (eds.), *Proceedings of the 35th International Conference on Machine Learning*, volume 80 of *Proceedings of Machine Learning Research*, pp. 284–293, Stockholm, Sweden, 10–15 Jul 2018b. PMLR. URL <http://proceedings.mlr.press/v80/athalye18b.html>.
- Carlini, N. and Wagner, D. Towards evaluating the robustness of neural networks. In *Security and Privacy (SP), 2017 IEEE Symposium on*, pp. 39–57. IEEE, 2017.
- Chizat, L., Peyré, G., Schmitzer, B., and Vialard, F.-X. Scaling algorithms for unbalanced transport problems. (2016). *arXiv preprint arXiv:1607.05816*, 2016.
- Croce, F., Andriushchenko, M., and Hein, M. Provable robustness of relu networks via maximization of linear regions. *CoRR*, abs/1810.07481, 2018. URL <http://arxiv.org/abs/1810.07481>.
- Cuturi, M. Sinkhorn distances: Lightspeed computation of optimal transport. In Burges, C. J. C., Bottou, L., Welling, M., Ghahramani, Z., and Weinberger, K. Q. (eds.), *Advances in Neural Information Processing Systems 26*, pp. 2292–2300. Curran Associates, Inc., 2013. URL <http://papers.nips.cc/paper/4927-sinkhorn-distances-lightspeed-computation-of-optimal-transport.pdf>.
- Dvijotham, K., Stanforth, R., Gowal, S., Mann, T., and Kohli, P. A dual approach to scalable verification of deep networks. In *Proceedings of the Thirty-Fourth Conference Annual Conference on Uncertainty in Artificial Intelligence (UAI-18)*, pp. 162–171, Corvallis, Oregon, 2018. AUAI Press.
- Engstrom, L., Tran, B., Tsipras, D., Schmidt, L., and Madry, A. A rotation and a translation suffice: Fooling cnns with simple transformations. *arXiv preprint arXiv:1712.02779*, 2017.
- Eykholt, K., Evtimov, I., Fernandes, E., Li, B., Rahmati, A., Xiao, C., Prakash, A., Kohno, T., and Song, D. Robust physical-world attacks on deep learning visual classification. In *Proceedings of the IEEE Conference on Computer Vision and Pattern Recognition*, pp. 1625–1634, 2018.
- Goodfellow, I., Shlens, J., and Szegedy, C. Explaining and harnessing adversarial examples. In *International Conference on Learning Representations*, 2015. URL <http://arxiv.org/abs/1412.6572>.
- Gowal, S., Dvijotham, K., Stanforth, R., Bunel, R., Qin, C., Uesato, J., Arandjelovic, R., Mann, T. A., and Kohli, P. On the effectiveness of interval bound propagation for training verifiably robust models. *CoRR*, abs/1810.12715, 2018. URL <http://arxiv.org/abs/1810.12715>.
- He, K., Zhang, X., Ren, S., and Sun, J. Deep residual learning for image recognition. In *Proceedings of the IEEE conference on computer vision and pattern recognition*, pp. 770–778, 2016.
- Jordan, R., Kinderlehrer, D., and Otto, F. The variational formulation of the fokker–planck equation. *SIAM journal on mathematical analysis*, 29(1):1–17, 1998.
- Kurakin, A., Goodfellow, I., and Bengio, S. Adversarial examples in the physical world. *ICLR Workshop*, 2017. URL <https://arxiv.org/abs/1607.02533>.
- Lu, J., Sibai, H., Fabry, E., and Forsyth, D. No need to worry about adversarial examples in object detection in autonomous vehicles. *arXiv preprint arXiv:1707.03501*, 2017.
- Madry, A., Makelov, A., Schmidt, L., Tsipras, D., and Vladu, A. Towards deep learning models resistant to adversarial attacks. In *International Conference on Learning Representations*, 2018. URL <https://openreview.net/forum?id=rJzIBfZAb>.
- Mirman, M., Gehr, T., and Vechev, M. Differentiable abstract interpretation for provably robust neural networks. In *International Conference on Machine Learning (ICML)*, 2018. URL <https://www.icml.cc/Conferences/2018/Schedule?showEvent=2477>.
- Papernot, N., McDaniel, P., Wu, X., Jha, S., and Swami, A. Distillation as a defense to adversarial perturbations against deep neural networks. In *Security and Privacy (SP), 2016 IEEE Symposium on*, pp. 582–597. IEEE, 2016.
- Peleg, S., Werman, M., and Rom, H. A unified approach to the change of resolution: Space and gray-level. *IEEE Transactions on Pattern Analysis and Machine Intelligence*, 11(7):739–742, 1989.

- Peyré, G. Entropic approximation of wasserstein gradient flows. *SIAM Journal on Imaging Sciences*, 8(4):2323–2351, 2015.
- Raghunathan, A., Steinhardt, J., and Liang, P. S. Semidefinite relaxations for certifying robustness to adversarial examples. In Bengio, S., Wallach, H., Larochelle, H., Grauman, K., Cesa-Bianchi, N., and Garnett, R. (eds.), *Advances in Neural Information Processing Systems 31*, pp. 10900–10910. Curran Associates, Inc., 2018. URL <http://papers.nips.cc/paper/8285-semidefinite-relaxations-for-certifying-robustness-to-adversarial-examples.pdf>.
- Rubner, Y., Tomasi, C., and Guibas, L. J. The earth mover’s distance as a metric for image retrieval. *International journal of computer vision*, 40(2):99–121, 2000.
- Sharif, M., Bhagavatula, S., Bauer, L., and Reiter, M. K. Adversarial generative nets: Neural network attacks on state-of-the-art face recognition. *arXiv preprint arXiv:1801.00349*, 2017.
- Sinha, A., Namkoong, H., and Duchi, J. Certifying some distributional robustness with principled adversarial training. 2018.
- Snow, M. et al. Monge’s optimal transport distance for image classification. *arXiv preprint arXiv:1612.00181*, 2016.
- Szegedy, C., Zaremba, W., Sutskever, I., Bruna, J., Erhan, D., Goodfellow, I., and Fergus, R. Intriguing properties of neural networks. In *International Conference on Learning Representations*, 2014. URL <http://arxiv.org/abs/1312.6199>.
- Tjeng, V., Xiao, K. Y., and Tedrake, R. Evaluating robustness of neural networks with mixed integer programming. In *International Conference on Learning Representations*, 2019. URL <https://openreview.net/forum?id=HyGIIdiRqtm>.
- Wong, E. and Kolter, Z. Provable defenses against adversarial examples via the convex outer adversarial polytope. In *International Conference on Machine Learning*, pp. 5283–5292, 2018.
- Wong, E., Schmidt, F., Metzen, J. H., and Kolter, J. Z. Scaling provable adversarial defenses. In Bengio, S., Wallach, H., Larochelle, H., Grauman, K., Cesa-Bianchi, N., and Garnett, R. (eds.), *Advances in Neural Information Processing Systems 31*, pp. 8410–8419. Curran Associates, Inc., 2018. URL <http://papers.nips.cc/paper/8060-scaling-provable-adversarial-defenses.pdf>.
- Xiao, C., Zhu, J.-Y., Li, B., He, W., Liu, M., and Song, D. Spatially transformed adversarial examples. *arXiv preprint arXiv:1801.02612*, 2018.
- Xiao, K. Y., Tjeng, V., Shafiq, N. M. M., and Madry, A. Training for faster adversarial robustness verification via inducing reLU stability. In *International Conference on Learning Representations*, 2019. URL <https://openreview.net/forum?id=BJfIVjAcKm>.